Measurement of $1s2s\,^3S_1$–$1s2p\,^3P_{2,0}$ wavelengths in heliumlike phosphorus

D.J.H. Howie and J.D. Silver
Clarendon Laboratory, University of Oxford, Oxford OX1 3PU, United Kingdom

E.G. Myers
Department of Physics, Florida State University, Tallahassee, Florida 32306
(Received 1 July 1994; revised manuscript received 24 October 1994)

We have used photographic spectroscopy of a beam-foil source to perform a precision measurement of the vacuum ultraviolet $1s2s\,^3S_1$–$1s2p\,^3P_{2,0}$ transition wavelengths in heliumlike phosphorus. The results are 739.920 ± 0.025 Å and 813.32 ± 0.06 Å, respectively. This measurement constitutes a sensitive test of current relativistic and quantum electrodynamic calculations.

PACS number(s): 32.30.Jc, 31.30.Jv, 12.20.Fv

The $1s2s\,^3S_1$–$1s2p\,^3P_{2,0}$ transitions in the heliumlike system have been widely studied in recent years, both experimentally and theoretically. For the theorist, the heliumlike ion is of great significance, since it represents the simplest step towards a truly many-body system. The $1s2s\,^3S_1$–$1s2p\,^3P_{2,0}$ transitions are especially interesting because of the large relativistic and quantum electrodynamic (QED) contributions to the intervals. The present work is part of a series of precision measurements of these transitions for Z=14, 15, and 16 aimed at testing Z^4 corrections to the "benchmark" calculations of Drake [1] as discussed in Refs. [2–5].

This experiment was performed using the tandem Van de Graaff accelerator at Florida State University (FSU), and employed the same spectrometer and procedures as used in our previous measurements of these transitions in heliumlike silicon and sulfur [6,7]. The grating was set so that lines in the approximate wavelength range 550–920 Å would be imaged onto the film. The beam was of 76.5 MeV P^{8+} stripped and excited by a single 20 $\mu g\,cm^{-2}$ carbon foil. It was collimated to a width of 2.5 mm. The foil was located upstream of the spectrometer entrance slit so that only the first 2.7 mm of the beam after the foil was in view to the grating. The spectrograph was refocused for a fast beam using the method of Leavitt, Robson, and Stoner [8], with the film tilted to ensure that the whole range of wavelengths covered by the film was simultaneously correctly refocused [6]. The entrance slitwidth was set to 40 μm, slightly wider than the optimum value as extrapolated from the results of Leavitt *et al.* [8]. Kodak 101-01 film was used for the detection system. Two exposures were made at different accelerator beam times: F213, which was for a period of 26 h and a total accumulated charge after the target foil of 242 mC, and F306, for a period of 109 h and an accumulated charge of 910 mC. For only the second film was the weaker $^3P_0$ line dense enough on the film to be fitted.

The films were analyzed in Oxford using a specially modified Joyce-Loebl microdensitometer [9,10]. A characterization of the film was used to convert to VUV photon exposure levels [11]. The strongest lines in the densitized spectra were fitted with Gaussians of full width at half maximum of between 40 and 60 μm. The hyperfine structure of the lines of interest is not resolved. This is consistent with a calculation of the hyperfine splitting of

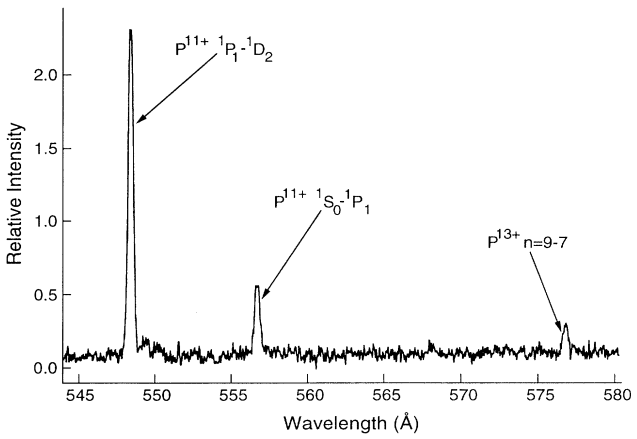

FIG. 1. Densitometer scan of a low-wavelength region of the phosphorus spectrum. The weak P^{13+} n=9-7 Rydberg line was omitted from the calibration curve.

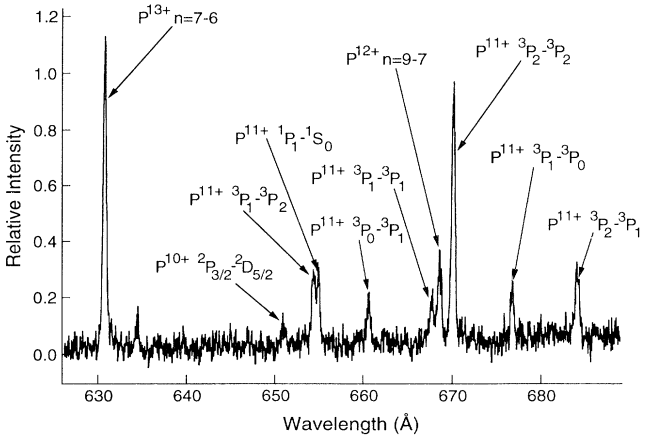

FIG. 2. Densitometer scan of a region of the spectrum containing one of the strong Rydberg lines together with lines of the berylliumlike ^3P-^3P multiplet.

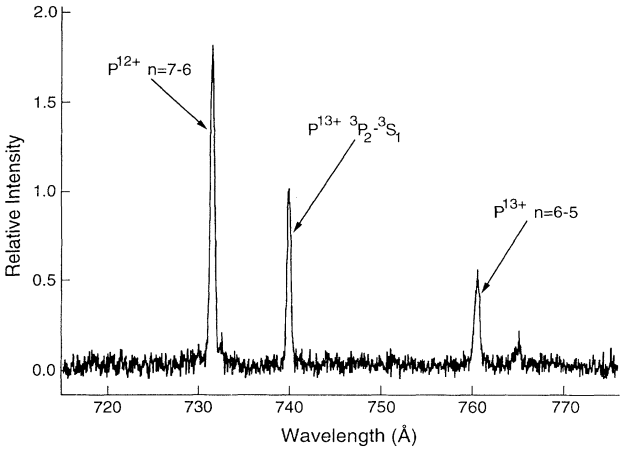

FIG. 3. Densitometer scan of a region of the spectrum showing the $^3P_2$ line of interest with two close-lying Rydberg lines.

the $^3P_2$ and $^3S_1$ levels using multiconfigurational Dirac-Fock (MCDF) wave functions [12], and also with a calculation using a simplified hyperfine Hamiltonian with nonrelativistic hydrogenic wave functions [13]. The MCDF calculation predicts a splitting between the two hyperfine components of $2\,^3S_1$ of 55 cm^{-1}. Typical linearized densitometer scans of the $F306$ film are presented in Figs. 1–4. The intensity of these scans is scaled relative to that of the $^3P_2$ line.

The spectra were calibrated using in-beam lines, of which the most important were from Rydberg transitions. Mean wavelengths and estimated uncertainties, appropriate to the conditions of observation, were obtained using the procedures of Ref. [6] and are listed in Table I. The uncertainty in the calculations of the wavelengths of the individual $n,l,j \rightarrow n',l',j'$ Rydberg components is believed to be < 0.001 Å and is negligible here. However, the observed Rydberg lines are blends of several closely spaced components with different upper-

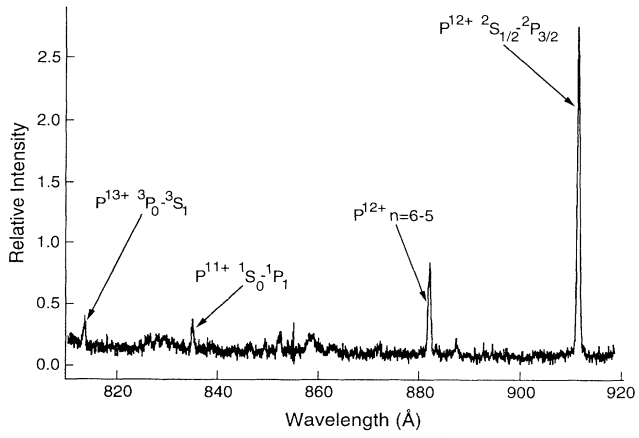

FIG. 4. Densitometer scan of the high-wavelength region of the spectrum. The $^3P_0$ line of interest can be seen towards the left-hand side of the scan.

TABLE I. Calculated mean wavelengths of identified Rydberg lines ($\beta = 0.073$, beam length viewed 0–2.70 mm from the foil).

	n'-n	λ (Å)	order
P^{13+}	7-6	630.720(7)	1
(He-like)	6-5	380.271(3)	2
	9-7	576.563(7)	1[a]
P^{12+}	7-6	731.510(7)	1
(Li-like)	6-5	441.044(3)	2
	9-7	668.693(7)	1

[a]Omitted from calibration curve, see text.

state lifetimes and the average wavelength is obtained from a cascade model. Uncertainties affecting the resulting observed mean wavelengths are the initial population distribution at the foil, the position of the region of the beam observed by the spectrometer with respect to the foil, and the effect of small asymmetries in the resulting blend when fitting a Gaussian profile. The combined error from these effects is indicated in Table 1. Lines from lower-lying transitions in the lithiumlike, berylliumlike, and boronlike systems were also used to verify the calibration, but with smaller weightings. The wavelengths of these lines have been previously measured, e.g., [14,15]. They can also be calculated from the semiempirical smoothed polynomial formulas of Edlén [16–22]. As these semiempirical values are expected to be more precise than the individual measurements, they were used in the calibration curves. The identified transitions, together with experimental and semiempirical wavelength values, are presented in Table II.

A first-order calibration curve was fitted to the plot of known wavelengths versus measured line centroids for the calibration lines. Because earlier work [10] with the same film stock and scanning techniques has shown residual errors for well known lines with a standard deviation of 0.01 Å, this error, combined with the line fitting errors, was used for the Rydberg lines when fitting the initial calibration curves. The errors in the modeled Rydberg wavelengths, as shown in Table I, were subsequently applied. This was done because the various effects that shift the modeled wavelengths affect all the Rydbergs in the same direction and are hence highly correlated. All of the Rydberg lines fitted well onto the calibration curve, with the exception of the two $\Delta n = 2$ transitions. The P^{12+} transition line shape was distorted, and had a large centroid fitting error. The P^{13+} line was weak, and was omitted from the fit. Edlén's wavelength values for non-Rydberg lines were indeed found to give a more consistent fit with the Rydberg lines and each other than the values from previous measurements. However, the effect of using these experimental values in the fit rather than Edlén's values only had a small effect (< 0.005 Å) on the extracted wavelengths of the lines of interest. Fitting a quadratic rather than a linear curve to the calibrations produced shifts of no more than 0.003 Å at the position of $^3P_2$ and 0.005 Å at the position of $^3P_0$.

The wavelengths and error budget of the lines of inter-

TABLE II. Identified transitions in ionized phosphorus.

Ion	Configuration	Term	J-J	Expt.[a]	SE[b]	Order
P^{12+} (Li-like)	$1s^2 2s$–$1s^2 2p$	^2S-^2P	$\frac{1}{2}$-$\frac{3}{2}$	455.67	455.766	2
P^{11+} (Be-like)	$1s^2 2s^2$-$1s^2 2s2p$	^1S-^1P	0-1	278.26	278.286	2,3
	$1s^2 2s2p$-$1s^2 2p^2$	^1P-^1D	1-2	548.38	548.35	1
		^1P-^1S	1-0		327.502	2
	$1s^2 2s2p$-$1s^2 2p^2$	^3P-^3P	2-1	342.02	342.050	2
			1-0	338.36	338.392	2
			2-2	335.02	335.078	2
			1-1	333.83	333.866	2
			0-1	330.21	330.324	2
			1-2	327.18	327.221	2
P^{10+} (B-like)	$2s^2 2p$-$2s2p^2$	^2P-^2D	$\frac{3}{2}$-$\frac{5}{2}$	325.51	325.525	2

[a]Experimental values from Kasyanov *et al.* [15], ±0.02 Å, except the ^1P–^1D value, which is from Fawcett [14], ±0.04 Å.

[b]Values from the semiempirical formalization of Edlén. Lithiumlike [16,20], berylliumlike [17,18], and [20] corrected according to [22], and boronlike [19,21].

est as obtained from the films are presented in Table III. The three contributions to the error budget are added in quadrature. The "line-shape fits" contribution is due to the centroid errors in fitting Gaussians to the lines of interest and is obtained from the fitting routine. Both of the lines of interest were fitted using single Gaussians. In addition, a composite two-Gaussian line shape was also fitted to the slightly asymmetric $^3P_0$ line. This composite line shape was constructed according to the calculated hyperfine component splitting and intensities, and provided a slightly better fit to the data than for the single Gaussian case. The centroid results from both profiles agreed to within their fitting errors. The "calibration" contribution consists of the combination of the standard deviations of the calibration curve for wavelengths at the lines of interest, which were 0.007 Å and 0.009 Å for $^3P_2$ and $^3P_0$, respectively, in film $F306$, and the effects of the uncertainties in the modeled Rydberg wavelengths shown in Table I. Of the total uncertainty due to the modeling of the Rydberg wavelengths, the uncertainty in the initial population model leads to an estimated contribution of 0.004 Å and 0.002 Å for the $^3P_2$ and $^3P_0$ lines, respectively, based on half the wavelength shift produced by assuming initial populations proportional to l^2 rather than $(2j+1)$ [6]. The uncertainties due to foil positioning and to asymmetry contribute respectively 0.004 Å and 0.003 Å to $^3P_2$, and 0.005 Å and 0.003 Å to $^3P_0$. The last contribution in Table III is the previously mentioned empirical error to account for imperfections in the microdensitometer scanning and various film effects such as nonuniform shrinkage.

The hyperfine effect leads to no appreciable shifts in the center of gravity of the levels, assuming a hyperfine component population proportional to the component multiplicity. (The negligible second-order effect is largest for the $^3P_0$ level, where it can be estimated to lead to an increase of the $^3S_1$-$^3P_0$ transition wavelength of about 0.001 Å.) Hyperfine quenching, an alteration in component decay rates due to hyperfine-induced mixing of states, has a small additional effect on the $^3P_2$ transition because of an additional $E1$ channel to the ground state opened to one of its components. The effect on the $^3P_2$ centroid leads to wavelength shifts of only a couple of thousandths of an angstrom [12].

Our final results are presented in Table IV. Because the weak $^3S_1$-$^3P_0$ line of interest appears on a single film, we have decided to increase the final quoted error to 0.06 Å, corresponding to a doubling of the fitting error presented in Table III. In the case of the $^3S_1$-$^3P_2$ line, we ensure redundancy by choosing the error of the less accurate measurement as the final quoted error. Our measurements are in good agreement with the results of [23] where a

TABLE III. Extracted wavelengths and error budget for the two films.

Source	$F213$	$F306$	
	$^3P_2$	$^3P_2$	$^3P_0$
Line-shape fits	0.010	0.003	0.030
Calibration	0.021	0.010	0.011
Scanning and film effects	0.010	0.010	0.010
Extracted wavelengths	739.91±0.025	739.920± 0.015	813.32 ± 0.033

TABLE IV. Results for P^{13+} $1s2s\,^3S_1$-$1s2p\,^3P_{2,0}$ wavelengths (Å).

Experimental	$^3P_2$	$^3P_0$
This work	739.920 ± 0.025	813.32 ± 0.06
Livingston and Hinterlong [23]	739.9 ± 0.1	813.4 ± 0.2
Theoretical		
MBPT [3]	739.913	813.306
Unified [1]	739.91	813.21
MCDF [24]	740.04	813.47
MCDF [25]	739.90	813.13

scanning monochrometer was used to observe a beam-foil source. As regards the theory the relativistic many-body perturbation theory (MBPT) values are seen to be in the best agreement with our work. These values can be taken from the work of Johnson and Sapirstein [3], or the "all-orders" work of Plante, Johnson, and Sapirstein [5], which yields near-identical results for this range of Z. Agreement is not so good with the MCDF methods [24,25], probably due to insufficient orbitals being included within these calculations to accurately account for electron-electron correlation.

The authors would like to thank the staff and students of the Florida State University Superconducting Accelerator Laboratory for enabling the running of the experiment, and Dr. J.H. Scofield for his calculation of the hyperfine effect. This work was supported in part by the National Science Foundation, the State of Florida, the U.K. Science and Engineering Research Council, and the Hasselblad Foundation.

[1] G.W.F. Drake, Can. J. Phys. **66**, 586 (1988).
[2] H.G. Berry, R.W. Dunford, and A.E. Livingston, Phys. Rev. A **47**, 698 (1993).
[3] W.R. Johnson and J. Sapirstein, Phys. Rev. A **46**, R2197 (1992).
[4] M.H. Chen, K.T. Cheng, and W.R. Johnson, Phys. Rev. A **47**, 3692 (1993).
[5] D.R. Plante, W.R. Johnson, and J. Sapirstein, Phys. Rev. A **49**, 3519 (1994).
[6] D.J.H Howie, W.A. Hallett, E.G. Myers, D.D. Dietrich, and J.D. Silver, Phys. Rev. A **49**, 4390 (1994).
[7] D.J.H. Howie, D. Phil. thesis, Oxford, 1994.
[8] J.A. Leavitt, J.W. Robson, and J.O. Stoner, Nucl. Instrum. Methods **110**, 423 (1973).
[9] J.S. Brown *et al.*, Nucl. Instrum. Methods Phys. Res. Sect. B **9**, 682 (1985).
[10] W.A. Hallett, D.D. Dietrich, and J.D. Silver, Phys. Rev. A **47**, 1130 (1993).
[11] W.M. Burton, A.T. Hatter, and A. Ridgeley, Appl. Opt. **12**, 1851 (1973).
[12] J.H. Scofield (private communication).
[13] H.A. Bethe and E.E. Salpeter, *Quantum Mechanics of One- and Two-Electron Atoms* (Plenum, New York, 1957).
[14] B.C. Fawcett, J. Phys. B **3**, 1152 (1970).
[15] Yu. S. Kasyanov *et al.*, Opt. Spektrosk. **35**, 1005 (1973). [Opt. Spectrosc. **35**, 586 (1973)].
[16] B. Edlén, Phys. Scr. **19**, 255 (1979).
[17] B. Edlén, Phys. Scr. **20**, 129 (1979).
[18] B. Edlén, Phys. Scr. **22**, 593 (1981).
[19] B. Edlén, Phys. Scr. **23**, 1079 (1981).
[20] B. Edlén, Phys. Scr. **28**, 51 (1983).
[21] B. Edlén, Phys. Scr. **28**, 483 (1983).
[22] B. Edlén, Phys. Scr. **32**, 86 (1985).
[23] A.E. Livingston and S.J. Hinterlong, Nucl. Instrum. Methods **202**, 103 (1982).
[24] P. Indelicato, Nucl. Instrum. Methods Phys. Res. Sect. B **31**, 14 (1988).
[25] J. Hata and I.P. Grant, J. Phys. B **16**, 523 (1983).